How Many-Body Correlations and α Clustering Shape ^{6}He

Carolina Romero-Redondo,[1,*] Sofia Quaglioni,[1,†] Petr Navrátil,[2,‡] and Guillaume Hupin[3,§]
[1]Lawrence Livermore National Laboratory, P.O. Box 808, L-414, Livermore, California 94551, USA
[2]TRIUMF, 4004 Wesbrook Mall, Vancouver, British Columbia V6T 2A3, Canada
[3]CEA, DAM, DIF, F-91297 Arpajon, France

(Received 1 June 2016; revised manuscript received 15 August 2016; published 23 November 2016)

The Borromean ^{6}He nucleus is an exotic system characterized by two halo neutrons orbiting around a compact ^{4}He (or α) core, in which the binary subsystems are unbound. The simultaneous reproduction of its small binding energy and extended matter and point-proton radii has been a challenge for *ab initio* theoretical calculations based on traditional bound-state methods. Using soft nucleon-nucleon interactions based on chiral effective field theory potentials, we show that supplementing the model space with $^4\mathrm{He}+n+n$ cluster degrees of freedom largely solves this issue. We analyze the role played by α clustering and many-body correlations, and study the dependence of the energy spectrum on the resolution scale of the interaction.

DOI: 10.1103/PhysRevLett.117.222501

Introduction.—Achieving a comprehensive and unified treatment of many-body correlations and clustering in atomic nuclei constitutes a frontier for contemporary nuclear theory. A light exotic nucleus that has been challenging our understanding of such complex phenomena based on nucleonic degrees of freedom and high-quality models of their interactions (i.e., within an *ab initio* framework) is helium-6 (^{6}He). This is a prominent example of Borromean quantum "halo," i.e., a weakly-bound state of three particles ($\alpha+n+n$) otherwise unbound in pairs, characterized by a "large probability of configurations within classically forbidden regions of space" [1]. In the last few years, its binding energy [2] and charge radius [3] have been experimentally determined with high precision. The ^{6}He ground state (g.s.) is also of great interest for tests of fundamental interactions and symmetries. Precision measurements of its β-decay half-life have recently taken place [4] and efforts are underway to determine the angular correlation between the emitted electron and neutrino [5]. To date, traditional *ab initio* bound-state calculations can successfully describe the interior of the ^{6}He wave function [6–10], but are unable to fully account for its three-cluster asymptotic behavior. At the same time, the only *ab initio* study of $\alpha+n+n$ dynamics naturally explains the asymptotic configurations, but underbinds the ^{6}He g.s. owing to missing many-body correlations [11,12]. As a result, a comprehensive description of the ^{6}He g.s. properties is still missing.

In this Letter we present a study of the ^{6}He g.s. in which both six-body correlations and clustering are successfully addressed by means of the no-core shell model with continuum (NCSMC) [13]. This approach, introduced to describe binary processes starting from two-body [14,15] and later three-body [16–18] Hamiltonians, is here generalized to the treatment of three-cluster dynamics. We further explore the role of six-body correlations in the description of the low-lying $\alpha+n+n$ continuum, required to accurately evaluate the $^4\mathrm{He}(2n,\gamma)^6\mathrm{He}$ radiative capture (one of the mechanisms by which stars can overcome the instability of the five- and eight-nucleon systems and create heavier nuclei [19]), and of the $^3\mathrm{H}(^3\mathrm{H},2n)^4\mathrm{He}$ reaction contributing to the neutron yield in inertial confinement fusion experiments [20,21].

Approach.—In the NCSMC, the A-nucleon wave function of a system characterized by a core $+n+n$ asymptotic in the total angular momentum, parity, and isospin channel $J^\pi T$ is written as the generalized cluster expansion

$$|\Psi^{J^\pi T}\rangle = \sum_\lambda c_\lambda^{J^\pi T}|A\lambda J^\pi T\rangle + \sum_\nu \iint dxdy x^2y^2 G_\nu^{J^\pi T}(x,y)\hat{\mathcal{A}}_\nu|\Phi_{\nu xy}^{J^\pi T}\rangle, \quad (1)$$

where $c_\lambda^{J^\pi T}$ and $G_\nu^{J^\pi T}(x,y)$ are, respectively, discrete and continuous variational amplitudes to be determined, $|A\lambda J^\pi T\rangle$ is the square-integrable (antisymmetric) solution for the λth energy eigenstate of the system obtained working within the A-body harmonic oscillator (HO) basis of the no-core shell model (NCSM) [22],

$$|\Phi_{\nu xy}^{J^\pi T}\rangle = [(|A-2\lambda_c J_c^{\pi_c} T_c\rangle(|n\rangle|n\rangle)^{(s_{nn}T_{nn})})^{(ST)} \times (Y_{\ell_x}(\hat{\eta}_{nn})Y_{\ell_y}(\hat{\eta}_{c,nn}))^{(L)}]^{(J^\pi T)} \times \frac{\delta(x-\eta_{nn})}{x\eta_{nn}}\frac{\delta(y-\eta_{c,nn})}{y\eta_{c,nn}} \quad (2)$$

are continuous microscopic-cluster states [11] describing the organization of the nucleons into an $(A-2)$-nucleon core and two neutrons $|n\rangle$, and the intercluster antisymmetrizer $\hat{\mathcal{A}}_\nu$ enforces the Pauli principle. The core eigenstates are also computed in the NCSM, with the same HO frequency $\hbar\Omega$ and consistent number of quanta above the lowest-energy configuration $N_{\max}$ used for the A-nucleon system. The states of Eq. (2) are labeled by the quantum numbers $\nu=\{A-2\lambda_c J_c^{\pi_c} T_c; s_{nn} T_{nn} S \ell_x \ell_y L\}$. Furthermore,

$\vec{\eta}_{c,nn} = \eta_{c,nn}\hat{\eta}_{c,nn}$ and $\vec{\eta}_{nn} = \eta_{nn}\hat{\eta}_{nn}$ are coordinates proportional to the separation between the centers of mass (c.m.s) of the core and residual two neutrons, and to the neutrons' relative position, respectively.

Similar to the binary-cluster case [15], upon orthogonalization of expansion (1), we obtain the unknown $c_\lambda^{J^\pi T}$ and $G_\nu^{J^\pi T}(x,y)$ amplitudes by solving the Schrödinger equation in the model space spanned by the basis states $|A\lambda J^\pi T\rangle$ and $\mathcal{A}_\nu|\Phi_{\nu xy}^{J^\pi T}\rangle$. However, given the additional relative coordinate, in the three-cluster case we first express the continuous amplitudes in the orthogonalized expansion (i.e., the relative-motion wave functions) in terms of the hyperradius $\rho = \sqrt{x^2+y^2}$ and hyperangle $\alpha = \arctan x/y$ and expand them in the hyperangular basis $\phi_K^{\ell_x\ell_y}(\alpha)$ analogously to Ref. [11]. The ^{6}He g.s. energy and wave function $|\Psi_{\text{g.s.}}\rangle$, as well as the matrix elements of the $\alpha+n+n$ scattering matrix, are found by matching the orthogonalized form of expansion (1) with the known asymptotic behavior of the wave function using an extension of the microscopic R-matrix method on Lagrange mesh [15,23–27]. We obtain convergence of the hyperangular expansion and R-matrix method using the same parameters as in Refs. [11,12]. We then analyze the hyper-radial components of the $\alpha+n+n$ relative motion and preferred spatial configurations within the g.s. of ^{6}He. To this end, we perform a projection of $|\Psi_{\text{g.s.}}\rangle$ into the orthogonalized cluster basis (2), i.e.,

$$\sum_{\nu'}\iint dx'dy'x'^2y'^2\mathcal{N}^{-1/2}_{\nu\nu'}(x,y,x',y')\langle\Psi_{\text{g.s.}}|\hat{\mathcal{A}}_\nu|\Phi^{J^\pi T}_{\nu'x'y'}\rangle = \frac{1}{\rho^{5/2}}\sum_K \tilde{u}_{\nu K}(\rho)\phi_K^{\ell_x\ell_y}(\alpha), \tag{3}$$

where $\mathcal{N}_{\nu\nu'}(x,y,x',y')$ is the overlap between the antisymmetrized states (2) [11]. Finally, we obtain the matter (r_m) and point-proton (r_{pp}) root-mean-square (rms) radii by computing the square root of the expectation values on the g.s. wave function of the operators

$$r_m^2 \equiv \frac{1}{A}\sum_{i=1}^{A} r_i^2 = \frac{1}{A}\rho^2 + \frac{A-2}{A}r_m^{2(c)}, \tag{4}$$

and

$$r_{pp}^2 \equiv \frac{1}{Z}\sum_{i=1}^{A} r_i^2\frac{(1+\tau_i^{(z)})}{2} = r_{pp}^{2(c)} + R^{2(c)}, \tag{5}$$

respectively. Here Z is the total number of protons, $\tau_i^{(z)}$ is the third component of isospin and r_i the distance from the A-nucleon c.m. of the ith nucleon, $r_m^{2(c)}$ and $r_{pp}^{2(c)}$ are core operators defined analogously to Eqs. (4) and (5), respectively, and $R^{(c)} = \sqrt{2/A(A-2)}\eta_{c,nn}$ is the distance between the c.m. of the core and that of the whole system. The expressions on the far right-hand side of Eqs. (4) and (5) are used to compute the matrix elements involving the microscopic-cluster portion of the basis and were specifically derived for core $+n+n$ partitions. In particular, the formulation of Eq. (5) is only valid for the present case of isospin $T_c = 0$ core. A more detailed account of the formalism will follow in a separate publication [28].

Results.—We start from the chiral next-to-next-to-next-to leading order (N^{3}LO) nucleon-nucleon (NN) interaction of Ref. [29] softened via the similarity renormalization group (SRG) method [30–32], which minimizes momentum components above a given resolution scale Λ, and disregard for the time being three-nucleon ($3N$) initial and SRG-induced components of the nuclear Hamiltonian. This defines a new NN interaction, unitarily equivalent to the initial potential in the two-nucleon sector only. In particular, we select $\Lambda = 2.0$ fm^{-1}. At this momentum resolution, the net effect of the (here disregarded) $3N$ forces tends to be suppressed in nuclei up to mass number $A = 6$, leading to binding energies close to experiment [33], and two- and higher-body SRG corrections to the ^{3}H and ^{4}He matter radii computed with bare operators have been shown to be negligible (less than 1%) [34]. In the interest of showcasing the vast improvement of the present approach over the use of expansions based exclusively on $\alpha+n+n$ microscopic-cluster states, we also perform calculations with the even softer $\Lambda = 1.5$ fm^{-1} resolution scale adopted in our earlier studies of Refs. [11,12]. Calculations for $\Lambda = 1.5$ and 2.0 fm^{-1} were carried out using the same $\hbar\Omega = 14$ and 20 MeV HO frequencies of Refs. [11,12] and [17], respectively. All results were obtained including only the $J_c^{\pi_c}T_c = 0^+0$ g.s. of the α particle and the first four, three, and two square-integrable eigenstates of the six-nucleon system for the $J^\pi = 0^+, 1^\pm$, and 2^+ channels, respectively. The effect of such truncation of the generalized cluster expansion (1) becomes negligible as the HO basis size increases, but can occasionally lead to a delayed onset of variational behavior. This can be seen, e.g., in the results for the ^{6}He g.s. energy, presented in Table I.

Convergence within the NCSMC is achieved within less than 10 keV for $\Lambda = 1.5$ fm^{-1}, in excellent agreement with

TABLE I. Computed ^{6}He g.s. energies in MeV for the $\Lambda = 1.5$ and 2.0 fm^{-1} interactions as a function of the absolute HO model space size $N_{\text{tot}} = N_0 + N_{\text{max}}$, where N_0 is the number of quanta shared by the nucleons in their lowest configuration. For the ^{4}He (g.s.) $+ n + n$ calculation of Ref. [11], $N_0 = 0$. However, for the p-shell ^{6}He nucleus within the NCSM and NCSMC, $N_0 = 2$. The last two rows show NCSM extrapolated results and the experimental value, respectively.

	$\Lambda = 1.5$ fm^{-1}			$\Lambda = 2.0$ fm^{-1}	
N_{tot}	Ref. [11]	NCSM	NCSMC	NCSM	NCSMC
6	−28.91	−27.71	−30.02	−26.44	−28.64
8	−28.62	−28.95	−29.69	−27.70	−28.81
10	−28.70	−29.45	−29.86	−28.37	−28.97
12	−28.70	−29.66	−29.86	−28.72	−29.17
∞	⋯	−29.84(4) [11]	⋯	−29.20(11) [8]	⋯
Expt.			−29.268		

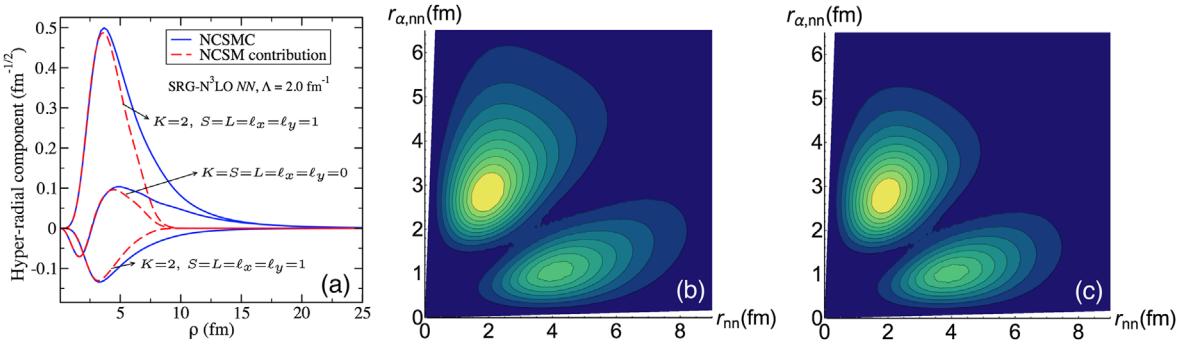

FIG. 1. (a) Most relevant hyper-radial components $\tilde{u}_{\nu K}(\rho)$ of the $\alpha + n + n$ relative motion [see Eq. (3)] within the ^{6}He g.s. after projection of the $\Lambda = 2.0$ fm^{-1} full NCSMC wave function in the largest model space (blue solid lines) as well as of its NCSM portion (red dashed lines) into the orthogonalized microscopic-cluster basis. (b),(c) Contour plots of the probability distribution obtained from the projection of the full NCSMC wave function of panel (a) and its NCSM component, respectively, as a function of the relative coordinates $r_{nn} = \sqrt{2}\eta_{nn}$ and $r_{\alpha,nn} = \sqrt{3/4}\eta_{\alpha,nn}$.

the infinite-space extrapolation of the NCSM [11]. Such a test, thanks also to accurate extrapolation techniques recently developed for NCSM g.s. energies [35–39], can be used to establish convergence of the NCSMC in more uncertain situations. This is the case for the harder ($\Lambda = 2.0$ fm^{-1}) interaction, where the good agreement with the extrapolated value of Ref. [8] is proof that results in the largest model space are close to convergence. The ^{4}He(g.s.) $+ n + n$ degrees of freedom efficiently account for the onset of clustering already in small model spaces. Conversely, the square-integrable eigenstates supply many-body correlations that are not accounted for in a microscopic-cluster expansion including only the g.s. of ^{4}He, such as the one shown in the first column of Table I (note that ^{6}He is unbound in the analogous calculations for $\Lambda = 2.0$ fm^{-1}). As shown in Fig. 1(a), the ^{4}He(g.s.) $+ n + n$ portion of the basis serves also the important role of providing the correct asymptotic behavior and extended configurations of the hyper-radial motion typical of a Borromean halo such as ^{6}He.

The projection over the orthogonalized microscopic-cluster basis of Eq. (3) captures 97% of the original NCSMC solution, confirming the $\alpha + n + n$ picture of the ^{6}He g.s. As shown in Fig. 1(b), similar to numerous previous studies [8,11,23,40–43] the "dineutron" configuration (two neutrons about 2 fm apart orbiting the core at a distance of about 3 fm) prevails over the "cigar" picture (two neutrons far from each other with the α particle in between). While these structures are already captured by the square-integrable portion of the basis [see Fig. 1(c)], they are more spatially extended in the full calculation.

The rms matter and point-proton radii obtained using the more "realistic" $\Lambda = 2.0$ fm^{-1} momentum resolution are shown together with the corresponding two-neutron separation energy (S_{2n}) in Fig. 2 and summarized in Table II. Also shown as shaded bands are the accurate S_{2n} measurement of Ref. [2], the range of experimental matter radii spanned by the values and associated error bars of Refs. [44–46], and the bounds for the point-proton radius as evaluated in Ref. [7] from the charge radius reported in Ref. [3]. All three observables exhibit a considerably

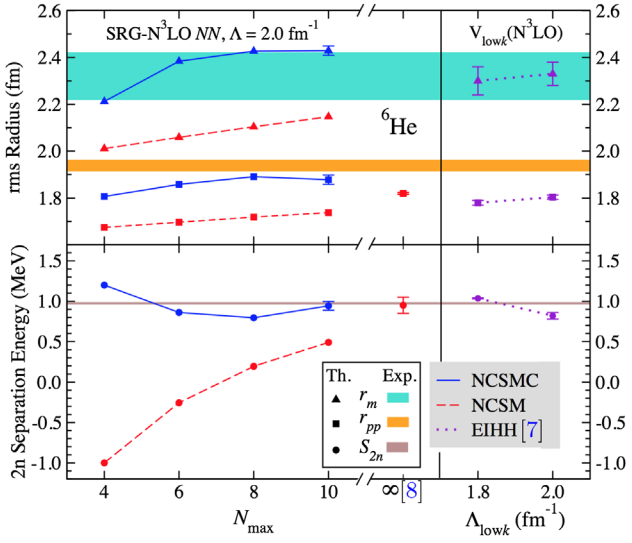

FIG. 2. NCSMC (blue solid lines) and NCSM (red dashed lines) rms matter (triangles) and point-proton (squares) radii, and two-neutron separation energy (circles), obtained using the SRG-N^{3}LO NN interaction with $\Lambda = 2.0$ fm^{-1} as a function of the HO basis size. Also shown are the infinite-basis extrapolations from Ref. [8] and the effective interaction hyperspherical harmonics (EIHH) results from Ref. [7] at the resolution scales $\Lambda_{\text{low}k} = 1.8$ and 2.0 fm^{-1}. The range of experimental values are represented by horizontal bands (see text for more details).

TABLE II. Summary of the results presented in Fig. 2, with $\Lambda_{\text{low}k}$ in units of fm^{-1}. See text for further details.

		S_{2n} (MeV)	r_m (fm)	r_{pp} (fm)
NCSMC	($N_{\max} = 10$)	0.94(5)	2.43(2)	1.88(2)
NCSM [8]	($N_{\max} = \infty$)	0.95(10)	⋯	1.820(4)
EIHH [7]	($\Lambda_{\text{low}k} = 2.0$)	0.82(4)	2.33(5)	1.804(9)
Expt.		0.975	2.32(10)	1.938(23)

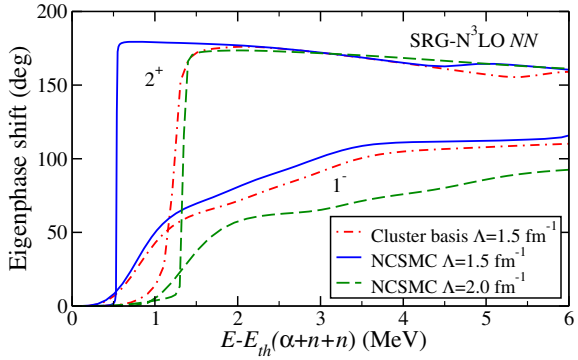

FIG. 3. Eigenphase shifts for channels 2^+ and 1^- as a function of the energy relative to the two-neutron emission threshold $E_{th}(\alpha + n + n)$ calculated with $\Lambda = 1.5$ fm^{-1} within the microscopic cluster basis (red dot-dashed lines) and NCSMC (blue solid lines), and $\Lambda = 2.0$ fm^{-1} within the NCSMC (green dashed lines).

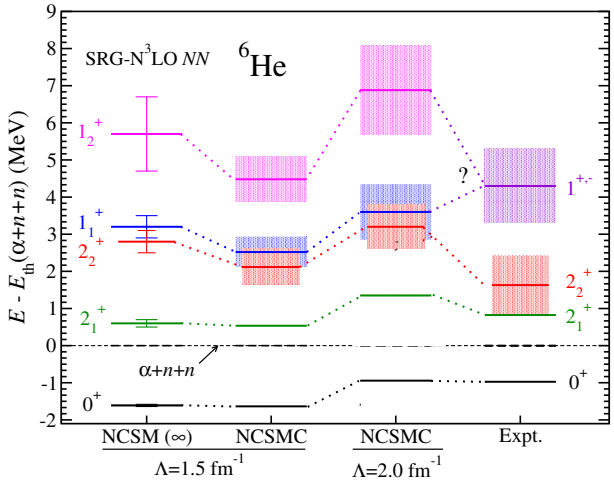

FIG. 4. Spectrum of ^{6}He. Results for $\Lambda = 1.5$ fm^{-1} are shown in the left for both NCSM and NCSMC. The third set of states corresponds to $\Lambda = 2.0$ fm^{-1} within the NCSMC and the fourth to the experimental spectrum [49]. See text for further details.

weaker dependence on the size of the HO basis compared to the results obtained within the NCSM (also shown in Fig. 2 as dashed red lines). An estimate of our uncertainties, based on both the convergence of the two-neutron emission threshold $E_{th}(\alpha + n + n)$ and the influence of ^{6}He square-integrable states beyond the g.s., is reported in Table II and shown in Fig. 2 for the largest model space. There, the theoretical S_{2n} is closest to its empirical value, and the computed r_m and r_{pp} radii are, respectively, at the upper end and just below the lower bound of their experimental bands. More interestingly, our point-proton radius is substantially larger than both the extrapolated value of Sääf *et al.*, which "calls for further investigations" [8], and the EIHH result of Bacca *et al.* [7]. This latter calculation, based on the $V_{\mathrm{low}k}(\mathrm{N^3LO})$ NN interaction, also yields a matter radius smaller than ours, though within the experimental bounds. The present combination of S_{2n} and r_{pp} values are more in line with the Green's function Monte Carlo results of Ref. [6], based on $NN + 3N$ forces constrained to reproduce the properties of light nuclei including ^{6}He.

With the present approach we are also able to quantify how the polarization of the α core affects the low-lying continuum of ^{6}He, a question that had been left unanswered by our previous study [12]. At the level of the $^4\mathrm{He} + n + n$ scattering eigenphase shifts obtained for the $\Lambda = 1.5$ fm^{-1} momentum resolution, the most significant effect is observed for the first $J^\pi = 2^+$ resonance, which becomes much sharper (with a width of $\Gamma = 15$ keV) and is shifted to lower energies (with the new centroid at 0.536 MeV). This behavior, indicative of a likely influence of the chiral $3N$ force on this state, can be seen in Fig. 3, which compares results obtained with (NCSMC) and without (cluster basis) coupling of ^{6}He square-integrable eigenstates. The effect in other partial waves is much more moderate. In particular, the 1^- eigenphase shift does not change significantly, excluding core-polarization effects as the possible origin of a low-lying dipole mode. A summary of the resonance centroids and widths (shown as shaded areas) extracted [47,48] from the computed $\Lambda = 1.5$ and 2.0 fm^{-1} positive-parity eigenphase shifts is presented and compared with experiment [49] in Fig. 4. Also shown, for the softer interaction, are extrapolated [50] energy levels (and their uncertainties) obtained within the NCSM by treating the ^{6}He excited states as bound states (note that the NCSM does not yield resonance widths). Clearly, such an approximation is only justified for the very narrow 2_1^+ resonance. The two SRG resolution scales produce a qualitatively similar picture, with the harder interaction leading to higher-lying and wider resonances (see also Fig. 3).

Conclusions.—We presented a comprehensive study of many-body correlations and α clustering in the g.s. and low-lying energy continuum of ^{6}He. While the inclusion of $3N$ forces (currently underway) remains crucial to restore the formal unitarity of the adopted SRG transformation of the Hamiltonian and arrive at an accurate description of the spectrum as a whole, the present results demonstrate that rms matter and point-proton radii compatible with experiment can be obtained starting from a soft NN interaction reproducing the ^{6}He small binding energy. A significant portion of the g.s. energy and the narrow width of the 2_1^+ resonance stem from many-body correlations that, in a microscopic-cluster picture, can be interpreted as core-excitation effects. In the future we plan to reexamine the *ab initio* calculation of the ^{6}He β-decay half-life, first carried out in Ref. [51], in the context of chiral effective field theory using wave functions with proper asymptotic behavior. This Letter also sets the stage for the *ab initio* study of the $^4\mathrm{He}(2n,\gamma)^6\mathrm{He}$ radiative capture and is a stepping stone in the calculation of the $^3\mathrm{H}(^3\mathrm{H}, 2n)^4\mathrm{He}$ fusion.

We thank J. Dohet-Eraly and A. Calci for multiple useful discussions and critical reading of the manuscript.

Computing support for this work came from the Lawrence Livermore National Laboratory (LLNL) institutional Computing Grand Challenge program, and from an INCITE Award on the Titan supercomputer of the Oak Ridge Leadership Computing Facility (OLCF) at Oak Ridge National Laboratory (ORNL). This Letter was prepared in part by LLNL under Contract No. DE-AC52-07NA27344. This material is based upon work supported by the U.S. Department of Energy, Office of Science, Office of Nuclear Physics, under Work Proposal No. SCW1158, and by the Natural Sciences and Engineering Research Council of Canada (NSERC) Grants No. 401945-2011 and No. SAPIN-2016-00033. TRIUMF receives federal funding via a contribution agreement with the National Research Council of Canada.

*romeroredond1@llnl.gov
†quaglioni1@llnl.gov
‡navratil@triumf.ca
§guillaume.hupin@cea.fr

[1] A. S. Jensen, K. Riisager, D. V. Fedorov, and E. Garrido, Rev. Mod. Phys. **76**, 215 (2004).
[2] M. Brodeur *et al.*, Phys. Rev. Lett. **108**, 052504 (2012).
[3] L.-B. Wang *et al.*, Phys. Rev. Lett. **93**, 142501 (2004).
[4] A. Knecht *et al.*, Phys. Rev. Lett. **108**, 122502 (2012).
[5] A. Garcia and O. Naviliat-Cuncic (private communication).
[6] S. D. Pieper, Riv. Nuovo Cimento Soc. Ital. Fis. **31**, 709 (2008).
[7] S. Bacca, N. Barnea, and A. Schwenk, Phys. Rev. C **86**, 034321 (2012).
[8] D. Sääf and C. Forssén, Phys. Rev. C **89**, 011303 (2014).
[9] M. A. Caprio, P. Maris, and J. P. Vary, Phys. Rev. C **90**, 034305 (2014).
[10] C. Constantinou, C. A. Caprio, J. P. Vary, and P. Maris, arXiv:1605.04976.
[11] S. Quaglioni, C. Romero-Redondo, and P. Navrátil, Phys. Rev. C **88**, 034320 (2013); **94**, 019902(E) (2016).
[12] C. Romero-Redondo, S. Quaglioni, P. Navrátil, and G. Hupin, Phys. Rev. Lett. **113**, 032503 (2014).
[13] P. Navrátil, S. Quaglioni, G. Hupin, C. Romero-Redondo, and A. Calci, Phys. Scr. **91**, 053002 (2016).
[14] S. Baroni, P. Navrátil, and S. Quaglioni, Phys. Rev. Lett. **110**, 022505 (2013).
[15] S. Baroni, P. Navrátil, and S. Quaglioni, Phys. Rev. C **87**, 034326 (2013).
[16] G. Hupin, S. Quaglioni, and P. Navrátil, Phys. Rev. C **90**, 061601 (2014).
[17] G. Hupin, S. Quaglioni, and P. Navrátil, Phys. Rev. Lett. **114**, 212502 (2015).
[18] J. Langhammer, P. Navrátil, S. Quaglioni, G. Hupin, A. Calci, and R. Roth, Phys. Rev. C **91**, 021301 (2015).
[19] F. Käppeler, F.-K. Thielemann, and M. Wiescher, Annu. Rev. Nucl. Part. Sci. **48**, 175 (1998).
[20] D. T. Casey *et al.*, Phys. Rev. Lett. **109**, 025003 (2012).
[21] D. B. Sayre *et al.*, Phys. Rev. Lett. **111**, 052501 (2013).
[22] P. Navrátil, J. P. Vary, and B. R. Barrett, Phys. Rev. C **62**, 054311 (2000).
[23] P. Descouvemont, C. Daniel, and D. Baye, Phys. Rev. C **67**, 044309 (2003).
[24] P. Descouvemont, E. Tursunov, and D. Baye, Nucl. Phys. **A765**, 370 (2006).
[25] D. Baye, J. Goldbeter, and J.-M. Sparenberg, Phys. Rev. A **65**, 052710 (2002).
[26] M. Hesse, J. Roland, and D. Baye, Nucl. Phys. **A709**, 184 (2002).
[27] M. Hesse, J.-M. Sparenberg, F. V. Raemdonck, and D. Baye, Nucl. Phys. **A640**, 37 (1998).
[28] C. Romero-Redondo, S. Quaglioni, P. Navrátil, and G. Hupin (to be published).
[29] D. R. Entem and R. Machleidt, Phys. Rev. C **68**, 041001 (2003).
[30] S. K. Bogner, R. J. Furnstahl, and R. J. Perry, Phys. Rev. C **75**, 061001 (2007).
[31] R. Roth, S. Reinhardt, and H. Hergert, Phys. Rev. C **77**, 064003 (2008).
[32] F. Wegner, Ann. Phys. (Leipzig) **506**, 77 (1994).
[33] E. D. Jurgenson, P. Navrátil, and R. J. Furnstahl, Phys. Rev. C **83**, 034301 (2011).
[34] M. D. Schuster, S. Quaglioni, C. W. Johnson, E. D. Jurgenson, and P. Navrátil, Phys. Rev. C **90**, 011301 (2014).
[35] S. A. Coon, M. I. Avetian, M. K. G. Kruse, U. van Kolck, P. Maris, and J. P. Vary, Phys. Rev. C **86**, 054002 (2012).
[36] R. J. Furnstahl, G. Hagen, and T. Papenbrock, Phys. Rev. C **86**, 031301 (2012).
[37] S. N. More, A. Ekström, R. J. Furnstahl, G. Hagen, and T. Papenbrock, Phys. Rev. C **87**, 044326 (2013).
[38] R. J. Furnstahl, S. N. More, and T. Papenbrock, Phys. Rev. C **89**, 044301 (2014).
[39] K. A. Wendt, C. Forssén, T. Papenbrock, and D. Sääf, Phys. Rev. C **91**, 061301 (2015).
[40] I. Brida and F. Nunes, Nucl. Phys. **A847**, 1 (2010).
[41] V. Kukulin, V. Krasnopolsky, V. Voronchev, and P. Sazonov, Nucl. Phys. **A453**, 365 (1986).
[42] M. Zhukov, B. Danilin, D. Fedorov, J. Bang, I. Thompson, and J. Vaagen, Phys. Rep. **231**, 151 (1993).
[43] E. Nielsen, D. Fedorov, A. Jensen, and E. Garrido, Phys. Rep. **347**, 373 (2001).
[44] I. Tanihata, D. Hirata, T. Kobayashi, S. Shimoura, K. Sugimoto, and H. Toki, Phys. Lett. B **289**, 261 (1992).
[45] G. D. Alkhazov *et al.*, Phys. Rev. Lett. **78**, 2313 (1997).
[46] O. Kiselev *et al.*, Eur. Phys. J. A **25**, 215 (2005).
[47] Centroids E_R and widths Γ are obtained, respectively, as the values of $E_{\rm kin} = E - E_{th(\alpha+n+n)}$ for which the first derivative $\delta'(E_{\rm kin})$ of the eigenphase shifts is maximal and $\Gamma = 2/\delta'(E_R)$.
[48] I. J. Thompson and F. M. Nunes, *Nuclear Reactions for Astrophysics* (Cambridge University Press, Cambridge, England, 2009), p. 301.
[49] X. Mougeot, V. Lapoux, W. Mittig, N. Alamanos, F. Auger *et al.*, Phys. Lett. B **718**, 441 (2012).
[50] Extrapolated values E_∞ are obtained from fitting the $N_{\rm max} = 6$ to 12 energies at $\hbar\Omega = 14$ MeV with the function $E(N_{\rm max}) = E_\infty + a\,\exp(-bN_{\rm max})$.
[51] R. Schiavilla and R. B. Wiringa, Phys. Rev. C **65**, 054302 (2002).